NASA TECHNICAL NOTE

N73-30865

NASA TN D-7308

NASA TN D-7308

CASE FILE COPY

CORRELATION OF NEW HYPERVELOCITY IMPACT DATA BY THRESHOLD PENETRATION RELATIONS

by Robert J. Hayduk, Paul S. Gough, and Emilio Alfaro-Bou

Langley Research Center
Hampton, Va. 23665

NATIONAL AERONAUTICS AND SPACE ADMINISTRATION • WASHINGTON, D. C. • SEPTEMBER 1973

1. Report No.	2. Government Accession No.	3. Recipient's Catalog No.
NASA TN D-7308		

4. Title and Subtitle	5. Report Date
CORRELATION OF NEW HYPERVELOCITY IMPACT DATA BY THRESHOLD PENETRATION RELATIONS	September 1973
	6. Performing Organization Code
7. Author(s)	8. Performing Organization Report No.
Robert J. Hayduk, Paul S. Gough, and Emilio Alfaro-Bou	L-8911
9. Performing Organization Name and Address	10. Work Unit No.
NASA Langley Research Center Hampton, Va. 23665	760-60-99-01
	11. Contract or Grant No.
12. Sponsoring Agency Name and Address	13. Type of Report and Period Covered
National Aeronautics and Space Administration Washington, D.C. 20546	Technical Note
	14. Sponsoring Agency Code

15. Supplementary Notes

Paul S. Gough is associated with Space Research Corp., North Troy, Vermont.

16. Abstract

Threshold penetration data are established by impacting spherical projectiles onto 2024 aluminum single-wall targets. Nylon and cadmium projectiles were used at impacting velocities from 3.0 to 6.8 km/s and 7.9 to 8.5 km/s, respectively. These data are combined with existing data and compared with three threshold penetration relations to assess their respective validities over a wide range of projectile densities (0.745 to 8.65 Mg/m^3). Two of these relations, one being the relation from NASA SP-8042, were validated over the extended range of projectile densities.

17. Key Words (Suggested by Author(s))	18. Distribution Statement
Hypervelocity impact Threshold penetration Ballistic limit	Unclassified – Unlimited

19. Security Classif. (of this report)	20. Security Classif. (of this page)	21. No. of Pages	22. Price*
Unclassified	Unclassified	29	Domestic, $3.00 Foreign, $5.50

*For sale by the National Technical Information Service, Springfield, Virginia 22151

CORRELATION OF NEW HYPERVELOCITY IMPACT DATA BY THRESHOLD PENETRATION RELATIONS

By Robert J. Hayduk, Paul S. Gough,* and Emilio Alfaro-Bou
Langley Research Center

SUMMARY

Threshold penetration data are established by impacting spherical projectiles onto 2024 aluminum single-wall targets. Nylon and cadmium projectiles were used at impacting velocities from 3.0 to 6.8 km/s and 7.9 to 8.5 km/s, respectively.

These data are combined with existing data and compared with three threshold penetration relations to assess their respective validities over a wide range of projectile densities (0.745 to 8.65 Mg/m^3). The relationships with projectile density to the 1/2 power and 0.519 power (recommended in NASA SP-8042) appear to be valid over the extended range of projectile densities considered in this investigation and may be used with confidence over this extended range. However, the 1/2-power relation has greater utilitarian value inasmuch as it correlates all the data with a single proportionality constant even though various target materials and examination techniques were used among the researchers to establish the data.

INTRODUCTION

One of the environmental hazards confronting a space vehicle is the possibility of penetration by a meteoroid. Studies of the environment indicate that the preponderance of meteoroids consists of extremely minute particles (ref. 1) traveling at very high velocities and in many cases the wall thickness established by structural requirements provide adequate armor protection. Critical areas of spacecraft are usually designed with a protective shroud or bumper which serves to fragment the meteoroid and spread the impulse of the debris over a much larger area on the main wall of the vehicle. However, some systems of spacecraft have requirements which preclude the use of a protective shroud or bumper. For example, waste-heat radiators of space power systems must be designed to resist penetration on the basis of armor (single-wall) considerations as the introduction of a protective shroud or bumper would interfere with the radiative efficiency.

---

*Space Research Corp., North Troy, Vermont.

Accordingly, the meteoroid penetration problem of a single wall has received substantial attention in the literature. The objective of the overall research activity is to provide the spacecraft designer with a reliable single-wall equation that he can incorporate into a design procedure. Several equations, which define the threshold of penetration in terms of target and projectile properties, have been presented in the literature. (See refs. 2 to 8.)

The primary objective of this paper is to assess the validity of three current threshold penetration relations over a wide range of projectile densities. For this purpose, new threshold penetration data, corresponding to both high and low projectile densities, will be presented. The facilities and techniques used to obtain these data will also be described.

SYMBOLS

d	projectile diameter, m
K_1	constant of proportionality (eq. (5))
m_p	projectile mass, kg
t	target thickness, m
V_p	projectile velocity, m/s
ϵ_t	target elongation, percent in 5 cm
ρ_p	projectile density, kg/m^3
ρ_t	target density, kg/m^3

THRESHOLD PENETRATION RELATIONS

Three current threshold penetration relations are considered in this paper. Two of these relations are modifications of an empirical relation presented in reference 2. The third is recommended in an NASA space vehicle design criteria document. (See ref. 7.)

In reference 2 Fish and Summers established the following empirical relation for the threshold of penetration:

$$\frac{t}{d} \propto \left(\frac{1}{\epsilon_t}\right)^{1/18} \frac{V_p}{\rho_t^{1/2}} \tag{1}$$

where t, ϵ_t, and ρ_t are the thickness, elongation (percent in 5 cm), and density, respectively, of the target and d and V_p are the projectile diameter and velocity, respectively. The penetration data of reference 2 were obtained by using 0.159-cm-diameter aluminum sphere projectiles and a variety of target materials. Expression (1) is essentially a relation between the projectile velocity and the target material properties, since no attempt was made to vary the projectile properties.

Theoretical analyses in references 4, 5, and 6 predicted that the proportionality

$$\frac{t}{d} \propto \frac{\rho_p}{\rho_t^{1/2}} V_p \tag{2}$$

would apply at the threshold of penetration. The ρ_p parameter is the projectile density. A linear relation between target thickness and impact velocity was also determined analytically in reference 3.

It is apparent that the empirical results confirmed the theoretical predictions for the dependences on impact velocity and target density. Hence, modification of equation (1), based upon theoretical analyses, results in the following relationship:

$$\frac{t}{d} \propto \left(\frac{1}{\epsilon_t}\right)^{1/18} \frac{\rho_p}{\rho_t^{1/2}} V_p \tag{3}$$

The experimental studies of reference 8 indicated that the target thickness at threshold penetration was proportional to the square root of projectile density. Accordingly, the empirical relation (1) of reference 2 was extended on an empirical basis in reference 8 to the following relation:

$$\frac{t}{d} \propto \left(\frac{1}{\epsilon_t}\right)^{1/18} \left(\frac{\rho_p}{\rho_t}\right)^{1/2} V_p \tag{4}$$

It should be noted that both expressions (3) and (4) contain an explicit dependence on the properties of the target. However, the NASA space vehicle design criteria document for meteoroid damage assessment (ref. 7) recommends the following equation to define the threshold of penetration for single-wall targets:

$$t = K_1 m_p^{0.352} \rho_p^{1/6} V_p^{0.875} \tag{5}$$

where specific values of K_1 are provided for several target materials. The constant K_1 for aluminum targets also depends upon the target examination technique used to determine the threshold penetration. Inasmuch as reference 7 considered only spherical projectiles, relationship (5) is recast to the form

$$\frac{t}{d} \propto d^{0.056} \rho_p^{0.519} V_p^{0.875} \tag{6}$$

so that it may be more readily compared with expressions (3) and (4).

References 2, 7, and 8 have established the validity of their respective relationships over a wide range of target material and impact velocities, but a relatively narrow range of projectile properties. Most of the data have been established with projectiles having densities between 2.26 and 2.79 Mg/m^3. The data of references 2, 8, and 9 are summarized in table I. It may be seen that no high-density data and only two low-density data points are included, namely, nylon (1.035 Mg/m^3) and Inlyte (0.745 Mg/m^3).

The data of table I are reinforced by five new data points obtained with nylon projectiles (1.14 Mg/m^3) and are extended by two new data points obtained with cadmium projectiles (8.65 Mg/m^3), presented in table II. This information permits an assessment of the three threshold penetration relations over a much wider range of projectile density.

EXPERIMENTAL FACILITIES

The new threshold penetration data presented in this paper were obtained in two facilities; these facilities are described in appendixes A and B. The lithium-hydride exploding foil facility at NASA Langley Research Center has been used to generate data with nylon spheres, and the light gas gun facility of the Space Research Corporation has been used to establish data with cadmium spheres.

The lithium hydride gun operates very simply – the energy stored in a capacitor bank is used to explode a short piece of aluminum foil surrounded by lithium hydride powder. The decomposed lithium hydride produces a high-pressure plasma which propels the projectile, a nylon sphere or slug. The projectile, traveling in an evacuated chamber, passes through a velocity recording system before impact on the target.

The light gas gun operates on the principle of repeated shock compression of hydrogen to provide a high-pressure driving gas which accelerates a saboted projectile. Upon exiting from the barrel, the sabot is separated from the projectile and prevented from impacting the target. A velocity recording system obtains in-flight information on projectile displacement, elapsed time, and integrity. The operational characteristics of the light gas gun are fairly standard; however, considerable time was spent in adjusting the gun parameters to meet the specific requirements of this test program.

DESCRIPTION OF NEW DATA

The data obtained with the facilities briefly described previously are presented in table II. They consist of five nylon projectile data points and two cadmium projectile

data points. Each of these data points was obtained by a bracketing process which involved several firings to determine the threshold of penetration. All targets were single walls made of 2024 aluminum.

Nylon Data

The nylon projectiles were spheres with nominal diameters of 0.159 cm, density of 1.14 Mg/m^3, and impact velocities from 3.0 to 6.8 km/s. Because of the high launch accelerations, deformation of the projectile was practically unavoidable. The photographs of figure 1 illustrate the range of deformation deemed to be acceptable by these investigators.

The targets used with the nylon projectiles were 7-cm-diameter 2024-T4 aluminum disks of various thicknesses. The photographs of figure 2 illustrate the no-penetration, threshold of penetration, and penetration conditions of impacted targets. All impacted targets were tested for penetration by means of a penetrant dye and by a standard laboratory helium leak detector at a pressure differential of 1 atmosphere. (1 atmosphere equals 0.1013 MN/m^2.) Both methods yielded the same results.

Typically, a series of targets at room temperature, all of the same nominal thickness, were impacted with nylon projectiles at various velocities. The object was to narrowly bracket the threshold of penetration with penetrations and no-penetrations. The velocities given in table II for the nylon data represent the average of a penetration and a no-penetration test.

Cadmium Data

The cadmium spheres launched by the light gas gun were nominally 0.318 cm in diameter with a density of 8.65 Mg/m^3. Two data points were established – 8.0 and 8.4 km/s. These cadmium data points were established by holding the projectile velocity relatively constant from shot to shot and varying the target thickness. The tolerances in table II indicate the bracketing range achieved. The penetration threshold was established by subjecting the target to a pressure differential of 1 atmosphere of air and checking for leaks.

The integrity of the cadmium projectiles was established just prior to impact by means of a flash X-ray photograph. Figure 3(a) shows an X-ray photograph of the projectile and also presents front and rear views of the 2.57-cm-thick target. The target held the pressure differential without leaking. The retention of shape illustrated by this projectile was typical of five of seven shots used to define the two data points. However, the two remaining shots involved deformed projectiles. The more deformed of these two projectiles is illustrated in figure 3(b) together with front and rear views of the target. The impact in this test involved a measured velocity of 8.0 km/s onto a target which was

2.22 cm thick. The target was tested under a pressure differential of 1 atmosphere and was found to leak.

Examination of figures 3(a) and 3(b) reveals pitting around the craters formed by the cadmium projectiles. This contamination of the target was due to the presence of sabot fragments. The degree of contamination illustrated was found to be unavoidable.

CORRELATION OF DATA BY THRESHOLD PENETRATION RELATIONS

In this section the degree of correlation of the data by expressions (3), (4), and (6) is examined. In what follows, the five nylon data points are grouped with existing data from table I and compared with the three threshold penetration relations. (See fig. 4.) This is done because the values of the correlating parameters associated with the nylon data fall within the range of the referenced data. Since the cadmium data essentially extend the range of the correlating parameters by a factor of two or four, the cadmium data are then compared (fig. 5) with the extrapolated least-squares line and lines of other slope defined subsequently. The data presented in figures 4 and 5 may be identified by reference to tables I and II.

Figure 4(a) presents the data correlated according to equation (3). The five new data points for nylon projectiles (⊢⊣) plus the nylon (■) and Inlyte (◆) data points of reference 8 do not cluster about the least-squares fit line as well as the other data of references 2, 8, and 9. The trend of these lower density projectile data points seems to be at a higher slope.

Figure 4(b) clearly reveals the improvement in the correlation of the data when the projectile density dependence is changed from ρ_p to $\rho_p^{1/2}$. (See eq. (4).) The low density projectile data points are brought into excellent agreement with both a least-squares fit line and the line from reference 8.

As reference 7 does not generalize the penetration relation (5) to an explicit dependence on target material properties, the data shown in figure 4(c) are all for aluminum targets. The pressure and visual criteria refer to the basis by which the threshold penetration was determined. These lines correspond to known values of the constant K_1 (eq. (5)) for aluminum alloy targets at room temperature as given in reference 7. The data point from reference 8 is the only one determined by a visual criterion, the others were established by a pressure criterion. The data fit both the least-squares fit and visual criterion lines very well, the pressure criterion line lying on the conservative side.

In figure 5(a) the cadmium data of table II are compared with the extrapolated least-squares fit of figure 4(a) and the poor correlation is evident. Since the velocity variation of the data is not extensive, the failure of expression (3) to correlate all the data is thought to be due to an incorrect projectile density dependence.

Similarly, in figures 5(b) and 5(c), the lines of figures 4(b) and 4(c) are extrapolated to compare with the cadmium data. The figures show a remarkable agreement between the extrapolated relations and the cadmium data. Both expressions (4) and (6) appear to be valid over the extended range of projectile densities considered in this paper (0.745 to 8.65 Mg/m^3). However, it can be seen by examining equations (4) and (6) that the dependence on projectile density is essentially the same. Expression (4) seems to have greater utilitarian value inasmuch as it correlates all the data with a single proportionality constant even though various target materials and examination techniques were used among the researchers to establish the data.

CONCLUDING REMARKS

An experimental investigation was made of the hypervelocity impact of spherical projectiles onto single-wall targets of 2024 aluminum. Threshold penetration data were established by using nylon projectiles at velocities between 3.0 and 6.8 km/s and with cadmium projectiles between 7.9 and 8.5 km/s. These data were combined with existing data from the literature and compared with three threshold penetration relations to assess their respective validities over a wide range of projectile density (0.745 to 8.65 Mg/m^3).

The relationship with the linear dependence on projectile density failed to correlate the data. Since this relationship arose from analytical consideration of certain simplified physical models of the hypervelocity impact phenomenon, the implication of the failure is that the models did not include all the principal mechanisms involved in the penetration process.

Both relationships with projectile density to the 1/2 power and 0.519 power (recommended in NASA SP-8042) appear to be valid over the extended range of projectile densities considered in this investigation and may be used with confidence over this extended range. However, the 1/2-power relation has greater utilitarian value inasmuch as it correlates all the data with a single proportionality constant even though various target materials and examination techniques were used among the researchers to establish the data.

Langley Research Center,
National Aeronautics and Space Administration,
Hampton, Va., May 29, 1973.

APPENDIX A

DESCRIPTION OF LITHIUM HYDRIDE GUN AND ASSOCIATED TECHNIQUES

The nylon-projectile data points presented in this paper were obtained by using a specially constructed launcher at Langley Research Center. The complete system and the techniques used to obtain hypervelocity impact data are described in this appendix.

The components of the lithium hydride gun are labeled in figure 6. The energy source consists of a 22-capacitor bank (two spares are shown, but are not in the circuit) having a total capacitance of 317 μF. Each capacitor has an average capacitance of $14\frac{1}{2}$ μF and is connected in parallel. The bank can be charged to 20 kV for a total energy of 63 400 joules. The energy level is varied depending on the projectile velocity required and the mass to be accelerated.

Figure 6 also shows the simple drop switch used to close the electrical circuit between the capacitor bank and the gun, the coil used to trigger the cameras and oscilloscope, the grounding switch, and power supply. The evacuated target chamber lies between two pairs of cameras and flash lamps. The barrel of the gun protrudes into the target chamber and the target is placed in a holder at the opposite end.

The lithium hydride gun (fig. 7) consists of a barrel, insulator breech, electrodes, and housing. The steel barrel is 7.6 cm long and has a tungsten-copper heat-resistant insert with a 0.159-cm-diameter polished bore. Barrels of shorter and longer lengths have been tried but no improvement in performance over the standard length could be observed. The projectile is a nylon sphere of 2.5 mg nominal mass and is inserted snugly in the breech end of the barrel.

The breech is made of aluminum oxide and has two holes forming a V-shaped path converging toward the barrel. A thin strip of aluminum foil placed in the V connects the electrodes. Lithium hydride, used as the propellant, is measured and poured into the two breech holes. The propellant gas is generated by an electric arc between the electrodes after the aluminum foil has exploded; as a result, the lithium hydride is decomposed and a high-pressure plasma is produced. At maximum available energy the projectile emerges at the muzzle end approximately 15 μs after the electric arc is initiated.

The carbon steel housing serves to maintain alinement and a vacuum seal between the barrel and breech, as well as to contain the high pressures and insulator fragments.

A schematic of the velocity measuring system is shown in figure 8. The system, which consists of two image converter tube cameras and two xenon-filled flash lamps, records the displacement of the projectile and its integrity during flight. The cameras

and an oscilloscope are triggered by the induced voltage in a coil located within the expanding magnetic field of the capacitor discharge circuit. This signal is fed into a time-delay generator in the cameras which causes the shutter to open at any time interval up to 100 μs after the initial signal is received. For longer times, an external time-delay generator is used. The time-delay generator is set to trigger the camera shutter at the instant in which the projectile passes within the camera field of view. This time has previously been obtained from a calibration curve of projectile velocity plotted against stored energy in the capacitor bank. The cameras send a signal to the oscilloscope when the shutter opens and the elapsed time between stations is recorded. The projectile velocity is calculated from the displacement of the projectile and the time interval between stations. (See fig. 8.)

APPENDIX B

DESCRIPTION OF LIGHT GAS GUN FACILITY AND ASSOCIATED TECHNIQUES

The cadmium-projectile data were generated by using the Space Research Corporation light gas gun. An external view of the light gas gun is presented in figure 9 and the internal geometry is illustrated in figure 10. The two chambers of the gun are initially filled with hydrogen at room temperature. The barrel is normally evacuated, together with the impact chamber, to a pressure of 1 torr (133.3 N/m^2). The driving pistons and the projectile are restrained by flanges during the load cycle. The breech of the gun is charged with a fast-burning small-arms propellant.

The propellant is ignited by a pyrotechnic squib and burns to drive the first piston forward in the first chamber, the hydrogen being compressed isentropically to approximately 300 MN/m^2. When the pressure in the first chamber develops to a sufficiently high level, the retaining flange of the second piston is either sheared or extruded. The second piston is accelerated forward vary rapidly in the short second chamber and a shock wave is developed. The shock is partially reflected at the tapered section of the chamber and partially transmitted into the barrel to initiate the motion of the projectile. The reflected portion of the shock wave will return to the piston face, be reflected and again overtake the projectile. It is estimated that as many as three or four reflected shock waves overtake the projectile during the launch cycle. The pressure in the volume between piston and projectile is raised by successive shock compressions to approximately 1.5 GN/m^2.

The internal ballistics of the light gas gun may be altered to the advantage of a particular program requirement by varying the propellant charge, the initial gas pressures, the weight of the pistons, and the diameter of the barrel. The values of these parameters were as follows: initial gas pressure in both chambers, 9 MN/m^2; quantity of propellant, 1 to 1.3 kg, depending on the velocity desired; first and second piston weights, 450 and 300 g, respectively.

The diameter of the barrel was chosen to be 1.27 cm. Since the projectile was a cadmium sphere having a diameter equal to 0.318 cm, it was necessary to utilize a sabot which would support the projectile during launch and seal against the driving gas. The sabot design used in the performance of this program is illustrated in figure 11. The magnesium core provided axial strength to the sabot during the launch together with radial support of the cadmium sphere. Obturation and resistance to initial motion were provided by the Lexan cup. A ring of material was removed from the front of the magnesium core and replaced by a Lexan ring in order to reduce weight. After assembly, a V-shaped groove was left in the front face. The purpose of this groove was to isolate the projectile,

as much as possible, from the effect of the device used to fracture and eliminate the sabot after the launch was completed.

Figure 12 illustrates the system used to separate the projectile from the sabot, the impact module, and the three flash X-ray units which were used to define the velocity and integrity of the projectile. A small quantity of silicon grease was introduced radially into the bore at two diametrically opposing locations. The grease decelerated the sabot and induced separation from the projectile. The sabot then impacted onto the heavy steel filter where a small hole permitted the projectile to pass through together with a small amount of debris from the sabot. After elimination of the sabot, the projectile traveled approximately 1 m into the impact module.

The condition of the projectile prior to entering the filter and after exiting was established by two 30 kV flash X-ray photographs, each having an exposure time of 100 ns. These cameras were triggered by detection of the sabot at the muzzle and were pulsed after a suitable preset delay. The time between the pulses was monitored on an oscilloscope. Figure 13 shows the three X-rays of shot 457. The fragments of the sabot are observed behind the projectile in the first image whereas the second shows the projectile isolated on the other side of the filter. From a measurement of the axial distance between the two images one may determine the axial travel of the projectile, and subsequently, the velocity. For the projectile of figure 13 the velocity was found to be 8.5 ± 0.1 km/s. Also shown in figure 13 is a third X-ray photograph which was used to establish the integrity of the projectile just prior to impact.

REFERENCES

1. Cosby, William A.; and Lyle, Robert G.: The Meteoroid Environment and Its Effects on Materials and Equipment. NASA SP-78, 1966.
2. Fish, Richard H.; and Summers, James L.: The Effect of Material Properties on Threshold Penetration. Proceedings of the Seventh Hypervelocity Impact Symposium, vol. VI, Feb. 1965, pp. 1-26. (Sponsored by U.S. Army, U.S. Air Force, and U.S. Navy.)
3. Thomson, Robert G.; and Kruszewski, E. T.: Effect of Target Material Yield Strength on Hypervelocity Perforation and Ballistic Limit. Proceedings of the Seventh Hypervelocity Impact Symposium, vol. V, Feb. 1965, pp. 273-320. (Sponsored by U.S. Army, U.S. Air Force, and U.S. Navy.)
4. Hayduk, Robert J.: Response of an Infinite Elastic Plate to Axisymmetric Initial Velocity Distributions With Application to Hypervelocity Impact. NASA TN D-5118, 1969.
5. Madden, Richard: Equations for the Comparison of the Ballistic Limit of Single and Double Wall Structures. Paper 69-370, AIAA Hypervelocity Impact Conference, Apr.-May 1969.
6. Weidman, Deene J.: Simplified Ballistic-Limit Expressions for Thin Sheets. NASA TN D-5556, 1969.
7. Frost, V. C.: Meteoroid Damage Assessment. NASA SP-8042, 1970.
8. Clough, Nestor; Lieblein, Seymour; and McMillan, Allen R.: Dimple, Spall, and Perforation Characteristics of Thin Plates of Nine Materials Under Hypervelocity Impact. NASA TN D-5625, 1970.
9. Swift, H. F.; Carson, J. M.; and Hopkins, A. K.: Ballistic Limits of 6061-T6 Aluminum Bumper Systems. AFML-TR-67-324, U.S. Air Force, Oct. 1967.
10. Anon.: Aluminum Standards & Data. First ed., Aluminum Association, Apr. 1968.

TABLE I. - SUMMARY OF THRESHOLD PENETRATION DATA FROM REFERENCES 2, 8, AND 9

Projectile material	Projectile density, ρ_p, Mg/m^3	Projectile diameter, d, cm	Projectile velocity, V_p, km/s	Target material	Target density, ρ_t, Mg/m^3	Target thickness, t, cm	Target material elongation, ϵ_t, percent	Symbols used in figure 3	Reference
2017-T4 aluminum	2.79	0.159	(a)	LA141A magnesium-lithium	1.35	(b)	10 to 20	◺	2
↓	↓	↓	↓	2024-T4 aluminum	2.768	↓	19	○	↓
				1100-0 aluminum	2.71		45	□	
				Armco 17-4PH stainless steel	7.78		6 to 15	◺	
				304 stainless steel	8.02		50	◻	
				Berylco 25 beryllium-copper	8.25		35 to 60	◇	
				Berylco 25 beryllium-copper	8.25		3 to 10	△	
Pyrex	2.26	.238	7.62	316 stainless steel	8.0	0.460	40	●	8
Nylon	1.035	.318	7.46	316 stainless steel	8.0	.432	40	■	↓
Inlyte	.745	.368	7.60	316 stainless steel	8.0	.432	40	◆	
Pyrex	2.26	.238	7.48	A-286	7.92	.501	18	▲	
↓	↓	↓	7.16	L-605	9.12	.456	35	◣	
			7.56	Inconel-718	8.20	.476	5	◣	
			7.62	2024-T6 aluminum	2.79	.829	7	◘	
	2.40	.318	7.62	Columbium-1-percent zirconium	8.05	.736	12	⬢	
	2.26	.238	7.62	Columbium-1-percent zirconium	8.05	.495	12	♦	
2017 aluminum	[c] 2.79	.318	[d] 6.715	6061-T6 aluminum	[c] 2.70	[d] 1.1290	[c] 17	◘	9

[a] Velocity in overall test program of reference 2 ranged from 0.5 to 8.5 km/s.

[b] Target thickness at penetration threshold not given explicitly in reference 2.

[c] Handbook values, reference 10.

[d] Average of perforation and no-perforation values given in reference 9.

TABLE II. - THRESHOLD PENETRATION DATA FROM IMPACT OF SPHERICAL PROJECTILES ONTO 2024 ALUMINUM SINGLE-WALL TARGETS

Projectile material	Projectile velocity, km/s	Target thickness, cm
Nylon*	3.14 ± 0.14	0.155 ± 0.001
Nylon	3.39 ± .17	.178 ± .001
Nylon	4.01 ± .04	.207 ± .001
Nylon	4.53 ± .08	.239 ± .001
Nylon	5.36 ± .20	.268 ± .001
Cadmium**	8.0 ± .1	2.37 ± .15
Cadmium	8.4 ± .1	2.54 ± .03

*Nylon data established by varying projectile velocity while holding target thickness constant. ($d = 0.159$ cm; $\rho_p = 1.14$ Mg/m^3; target material, 2024-T4 aluminum.)

**Cadmium data established by varying target thickness while holding projectile velocity nearly constant. ($d = 0.318$ cm; $\rho_p = 8.65$ Mg/m^3; target material, 2024-T3 aluminum.)

Undeformed Deformed

L-73-3075

Figure 1. - Examples of nylon projectile integrity.

No-penetration Threshold penetration Penetration

L-73-3076

Figure 2. - Photographs of target damage.

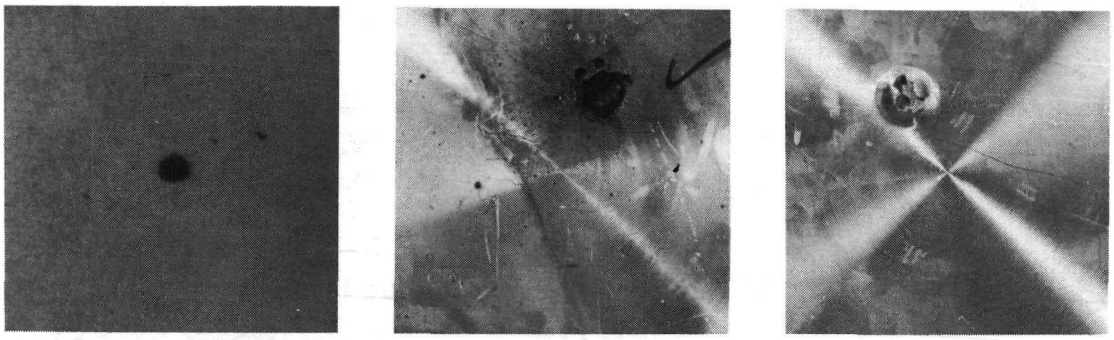

X-ray prior to impact | Front view | Rear view

(a) Velocity, 8.5 km/s.

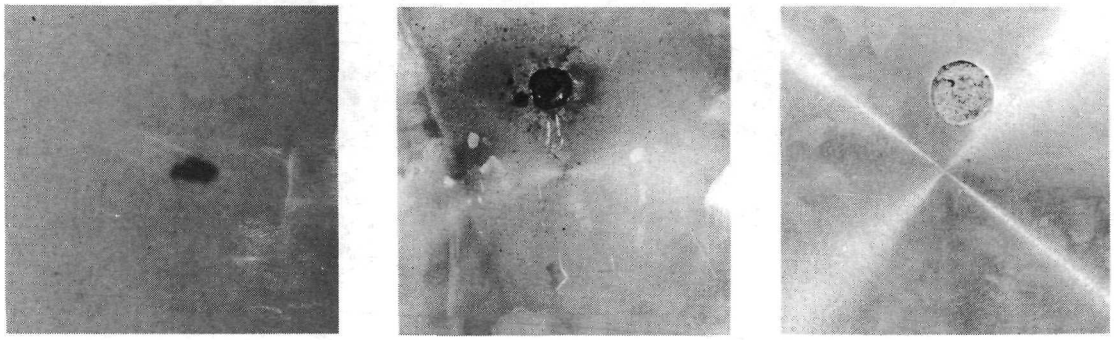

X-ray prior to impact | Front view | Rear view

(b) Velocity, 8.0 km/s.

L-73-3077

Figure 3.- Third X-ray photograph of cadmium projectile just prior to impact onto target together with front and rear views of the target.

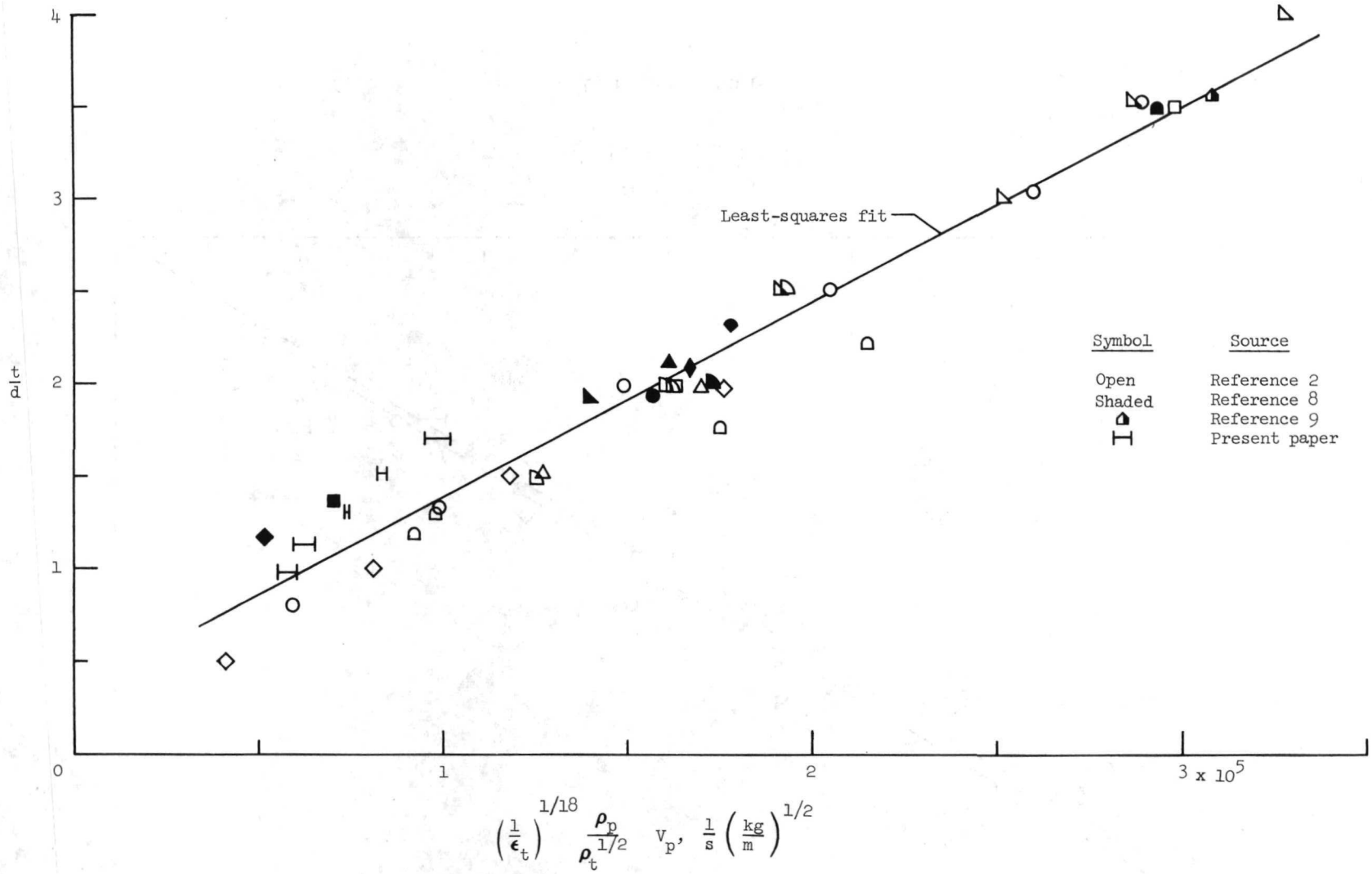

(a) Expression (3).

Figure 4.- Correlation of threshold penetration data. Projectile and target properties are identified in tables I and II.

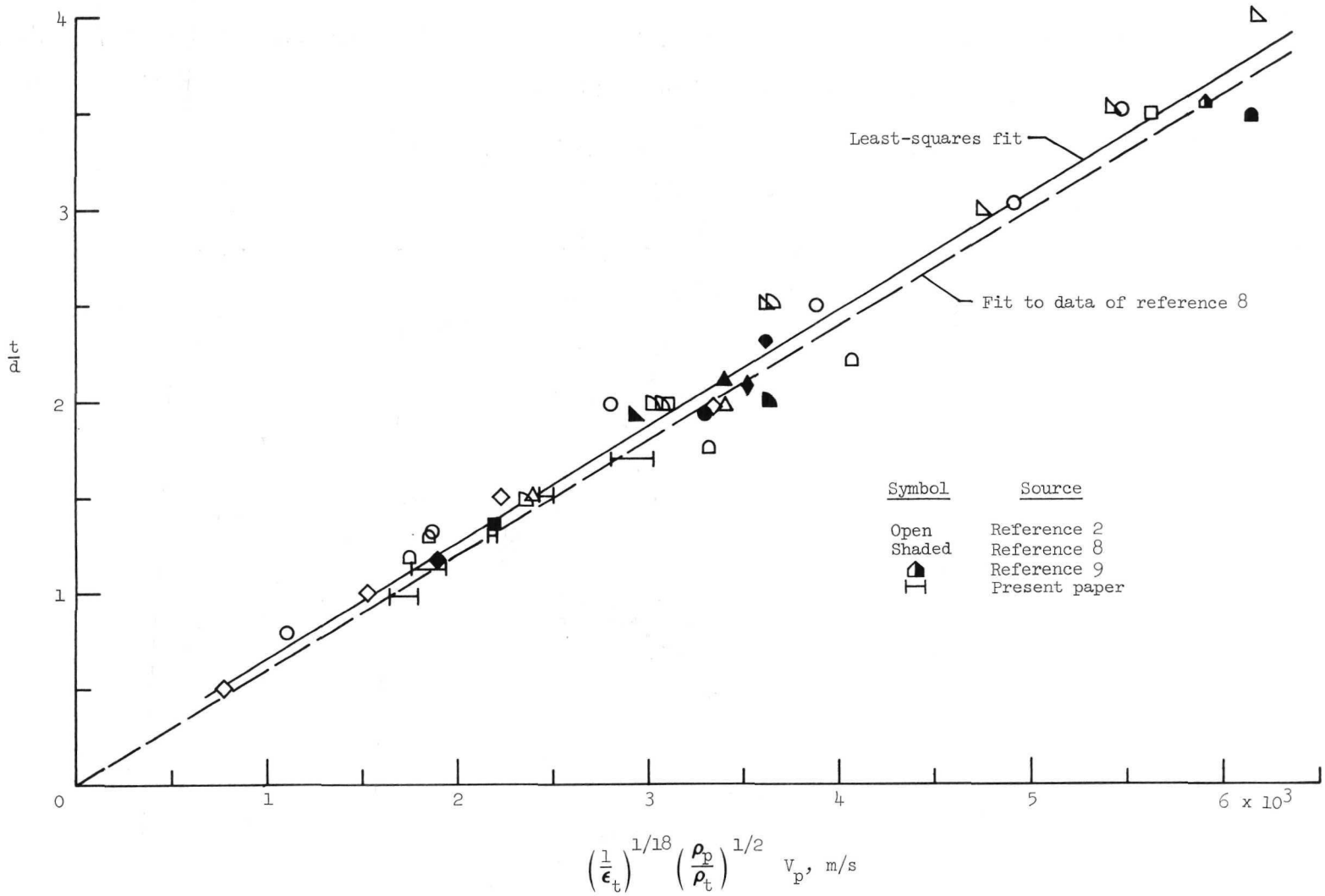

(b) Expression (4).

Figure 4.- Continued.

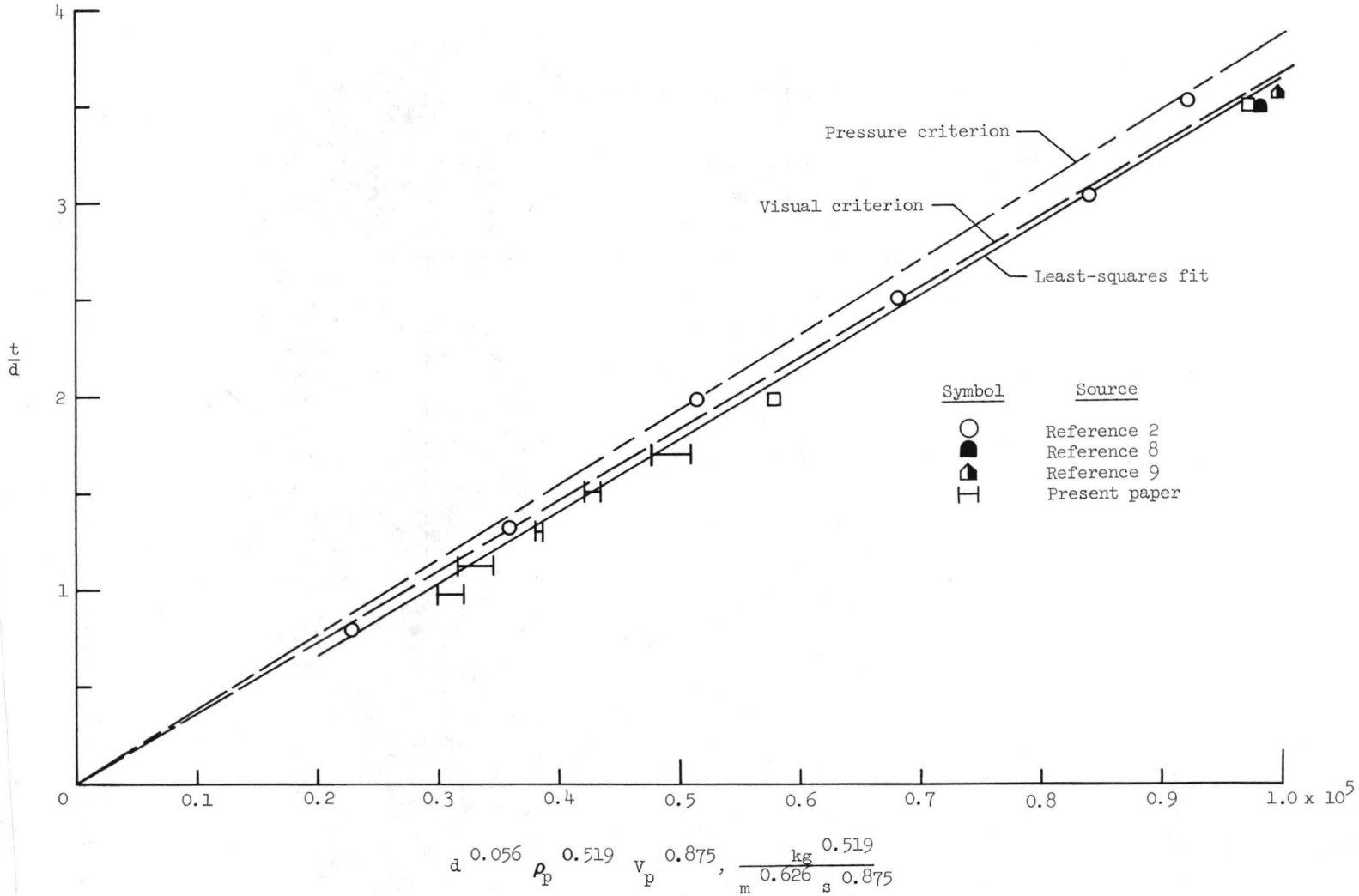

(c) Expression (6).

Figure 4.- Concluded.

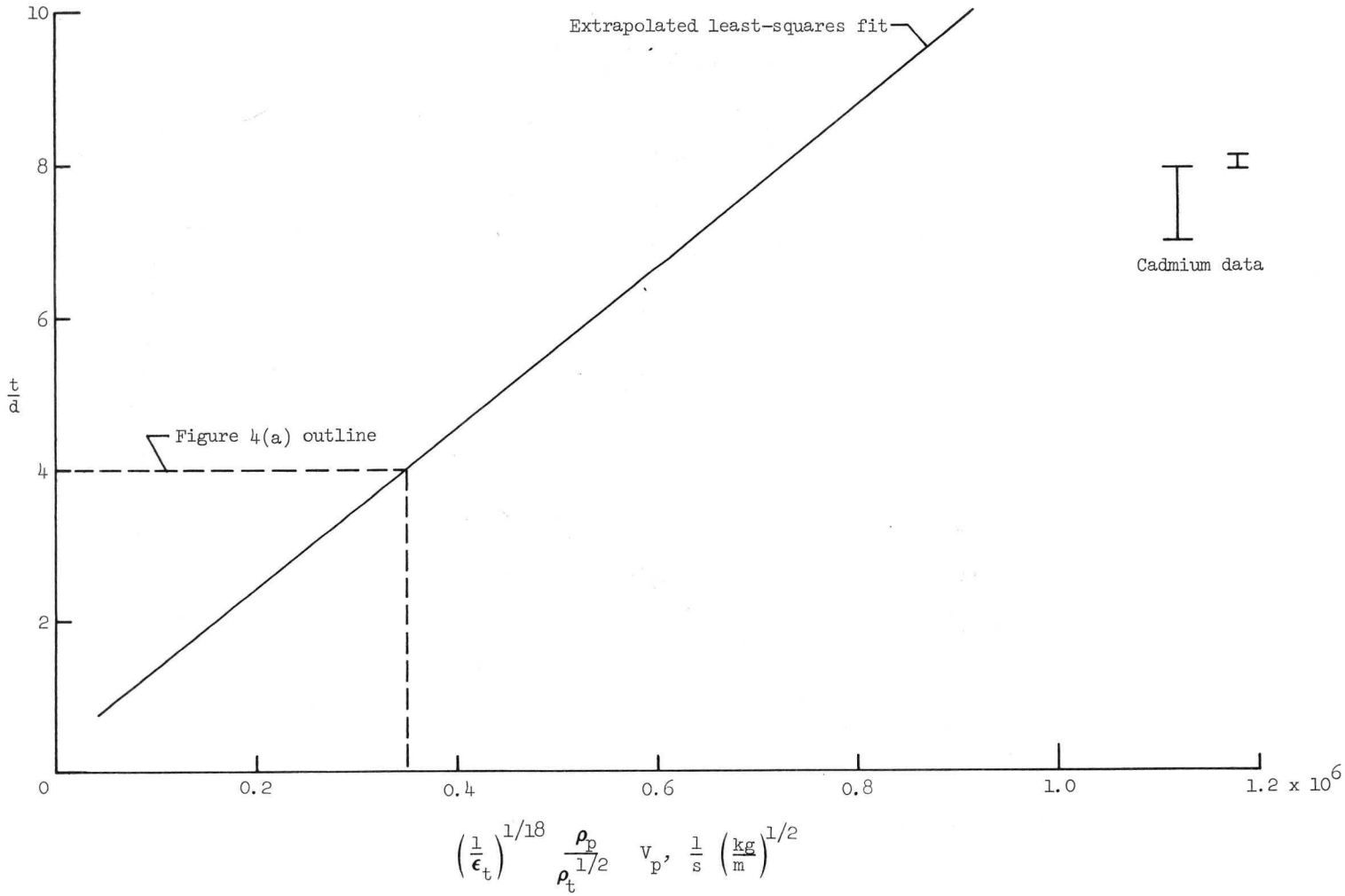

(a) Extrapolated expression (3).

Figure 5.- Correlation of cadmium data by extrapolated expressions.

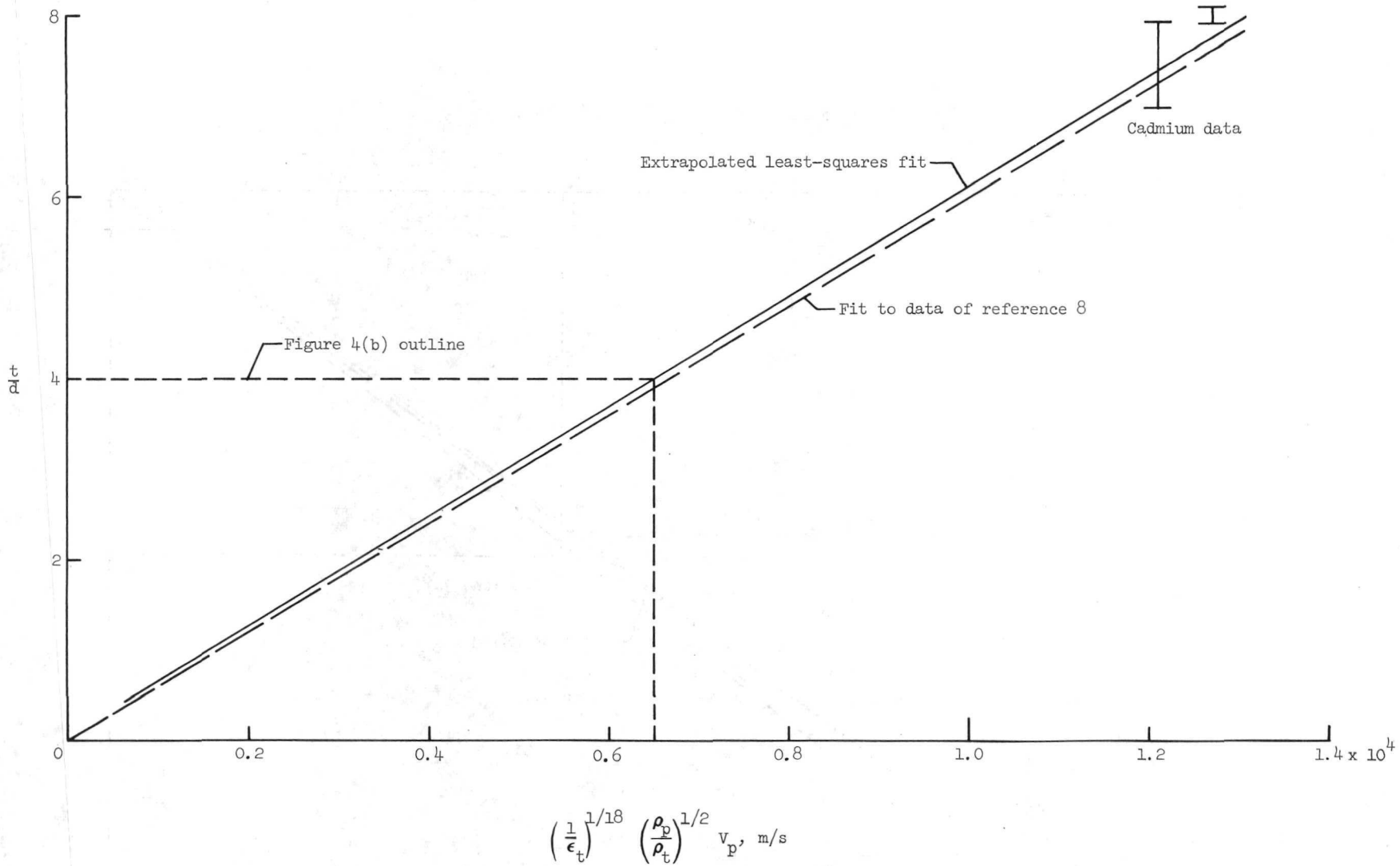

(b) Extrapolated expression (4).

Figure 5.- Continued.

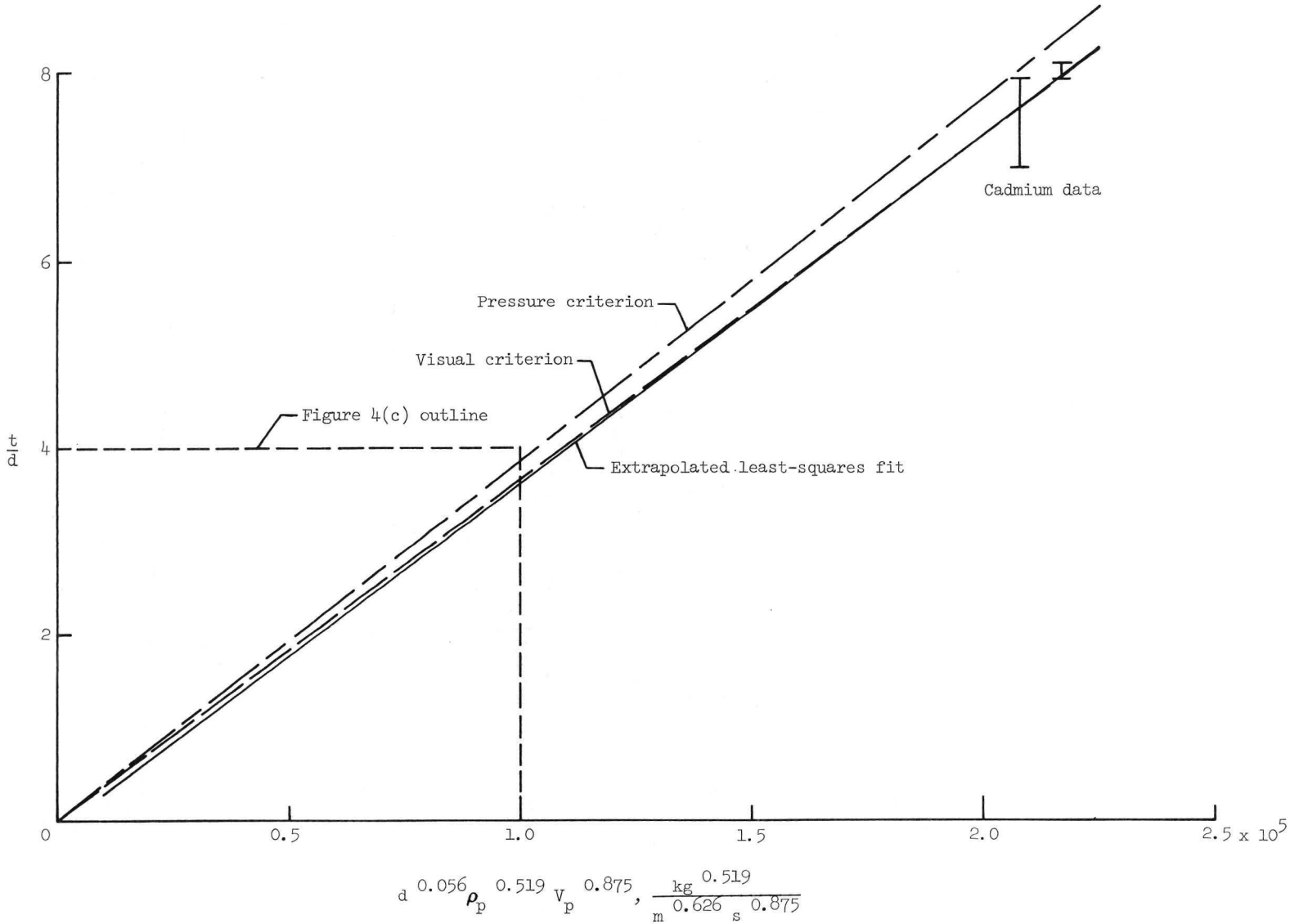

(c) Extrapolated expression (6).

Figure 5.- Concluded.

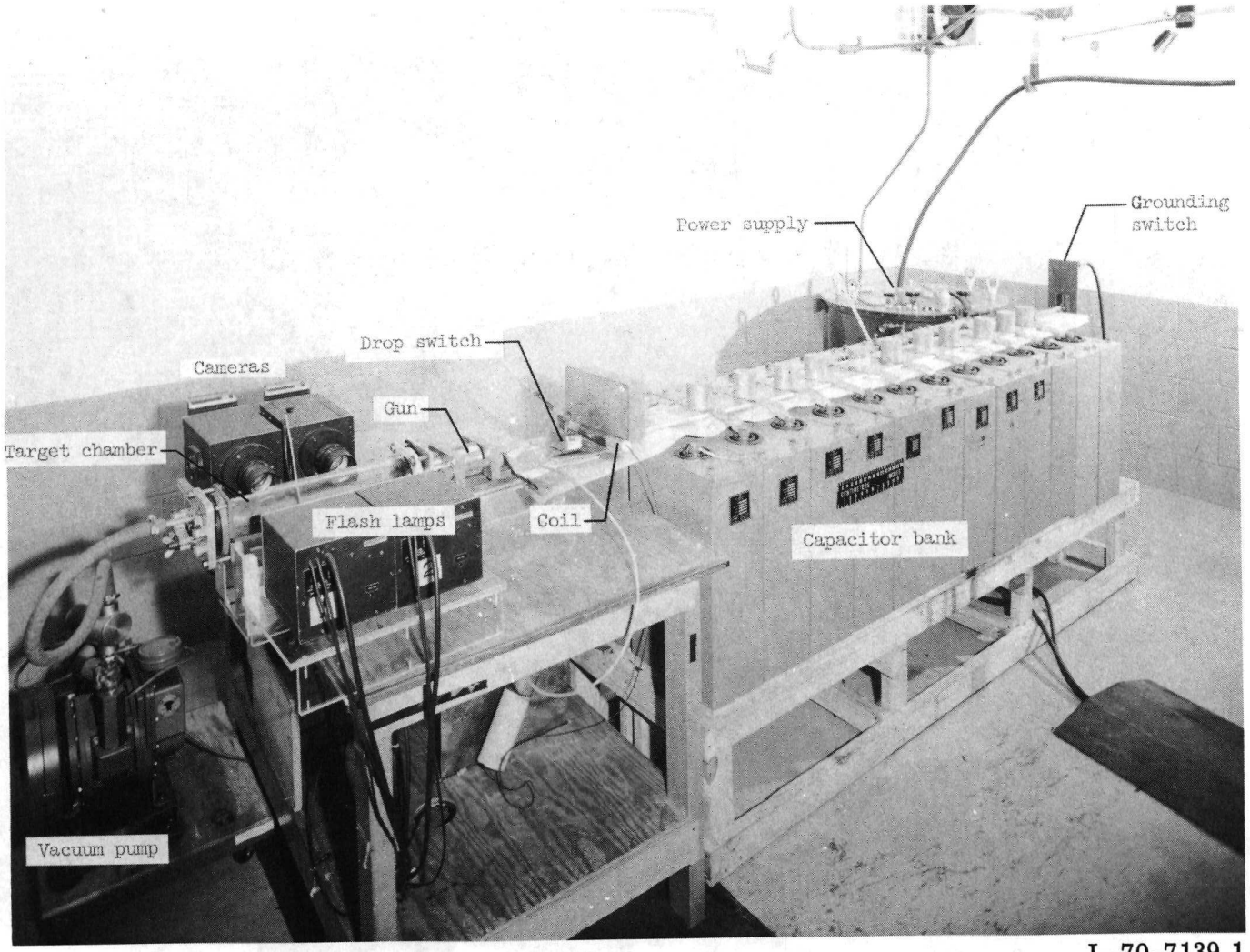

L-70-7139.1

Figure 6.- Lithium hydride gun.

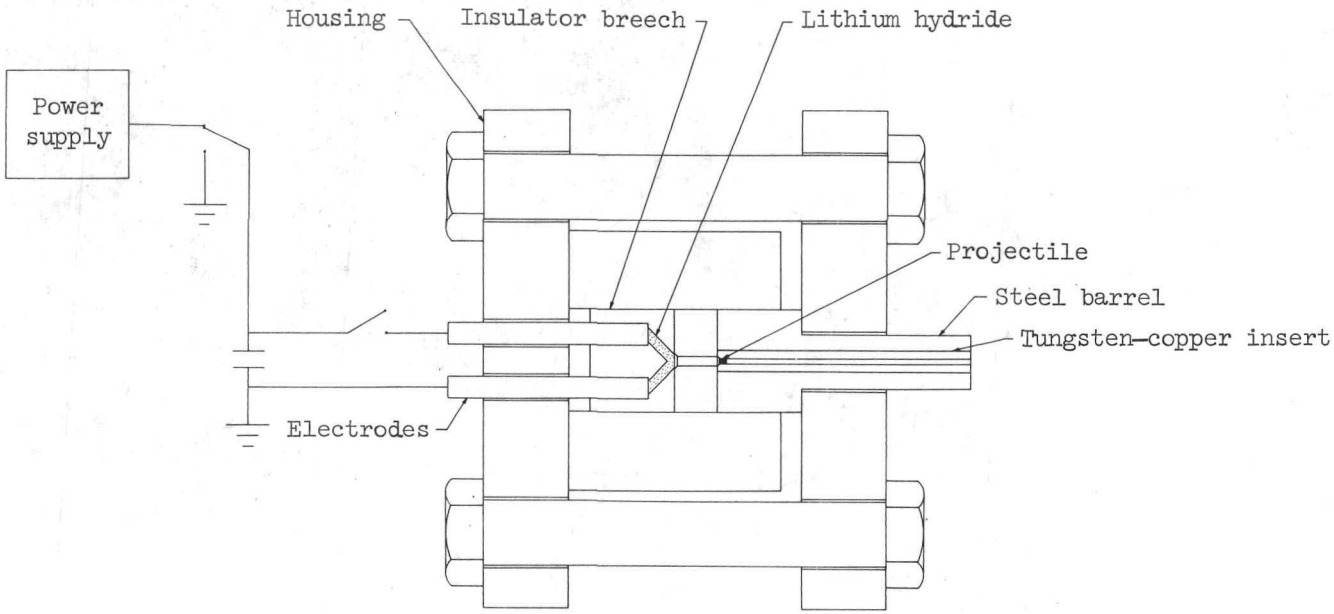

Figure 7.- Lithium hydride gun schematic.

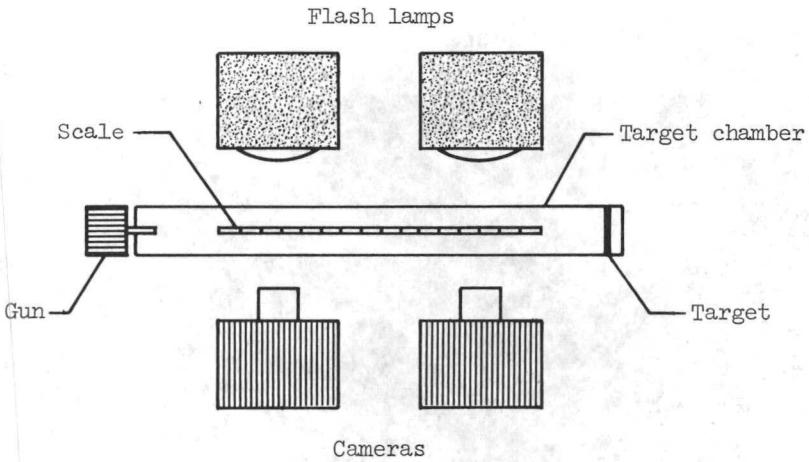

For impulse-type acceleration:

$$\text{Velocity} = \frac{\text{Displacement}}{\text{Elapsed time}} = \frac{18.5 \times 10^{-5}}{33 \times 10^{-6}} = 5.6 \text{ km/s}$$

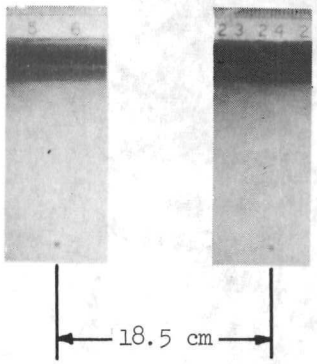

Projectile displacement

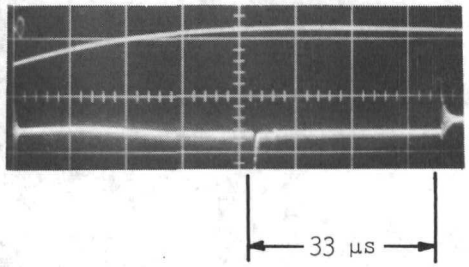

Oscilloscope trace

L-73-3078

Figure 8.- Nylon projectiles in flight and velocity-determination technique.

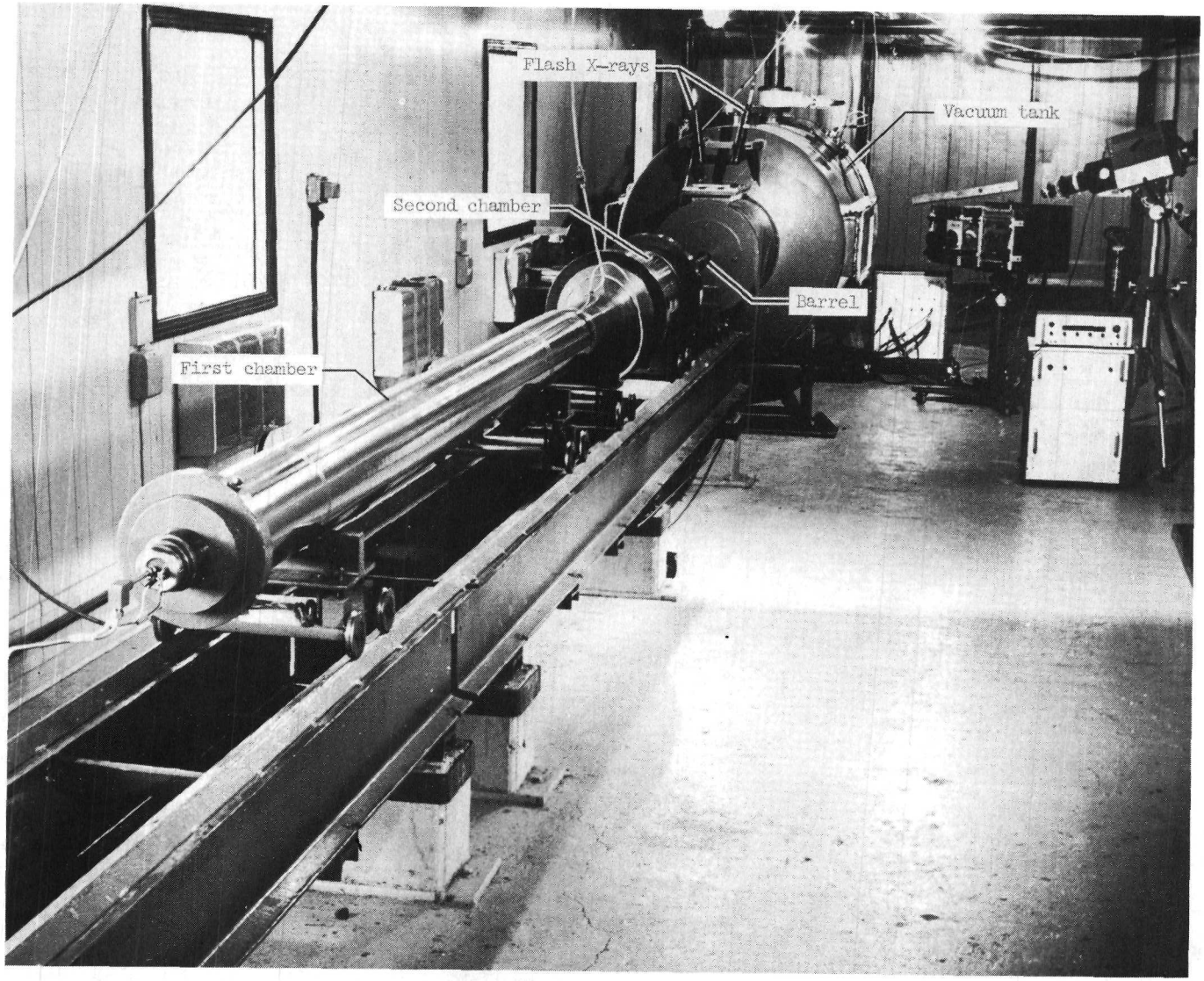

L-73-3079

Figure 9.- Space Research Corporation light gas gun.

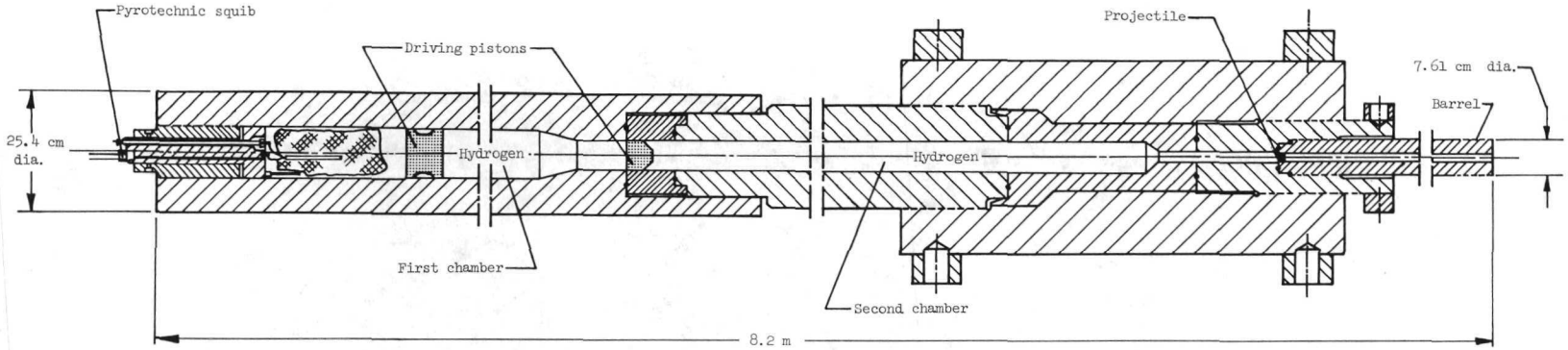

Figure 10.- Internal geometry of light gas gun.

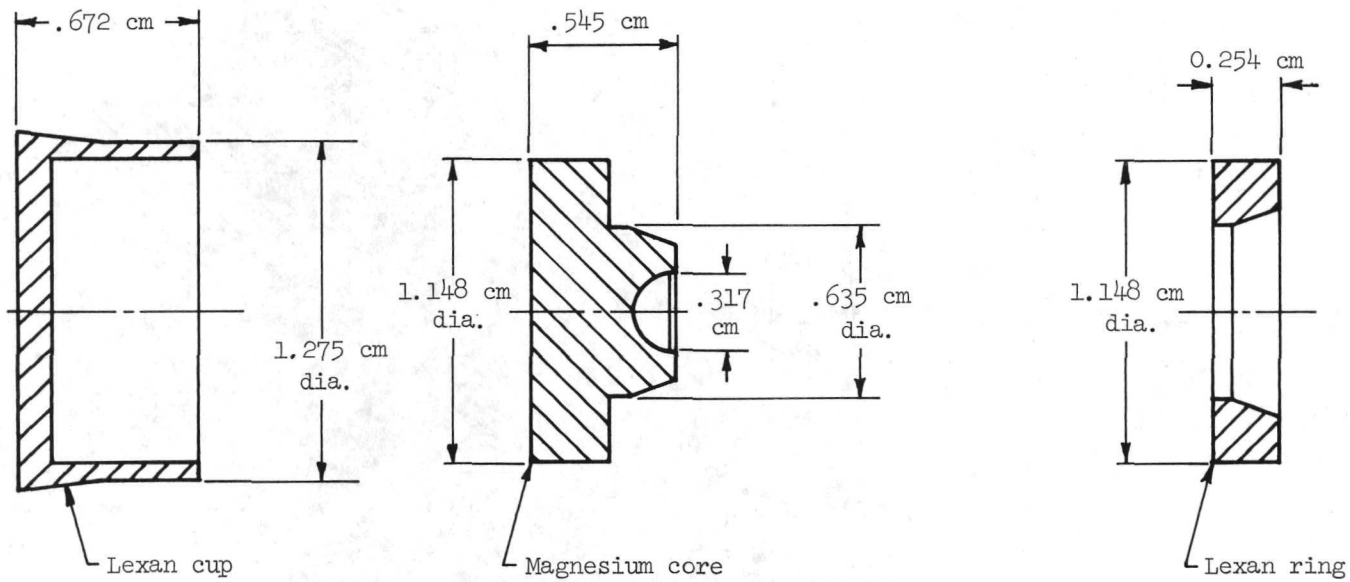

Figure 11.- Cross section of sabot components.

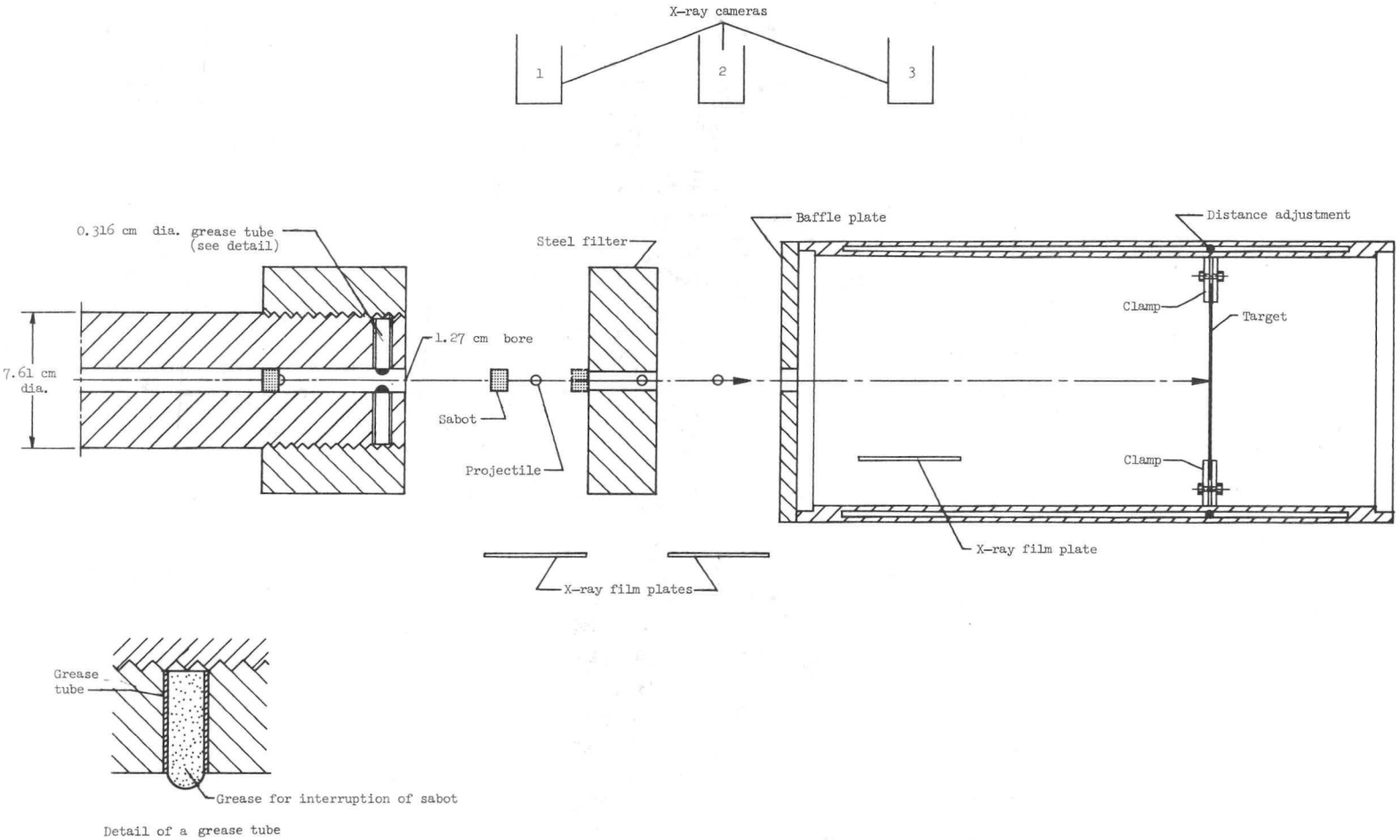

Figure 12.- Schematic of system used to isolate projectile from sabot and impact module.

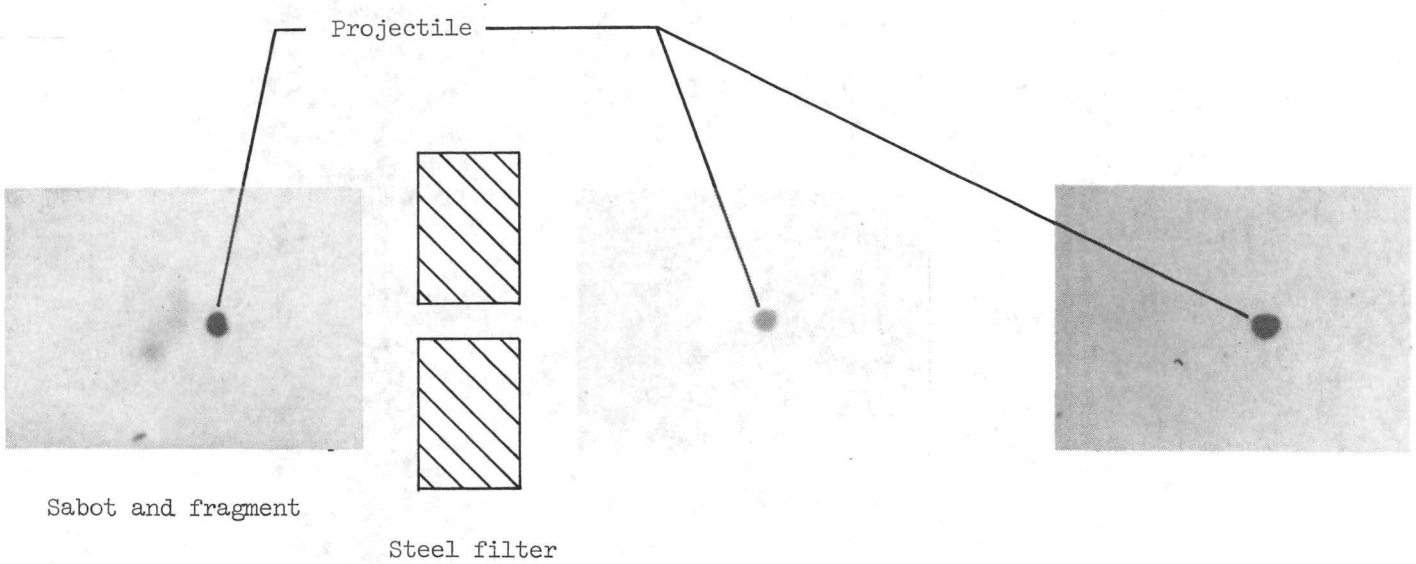

L-73-3090

Figure 13. - Three X-rays of projectile.

NASA-Langley, 1973 —— 32 L-8911

NATIONAL AERONAUTICS AND SPACE ADMINISTRATION
WASHINGTON, D.C. 20546

OFFICIAL BUSINESS
PENALTY FOR PRIVATE USE $300

SPECIAL FOURTH-CLASS RATE
BOOK

POSTAGE AND FEES PAID
NATIONAL AERONAUTICS AND
SPACE ADMINISTRATION
451

U.S.MAIL

POSTMASTER: If Undeliverable (Section 158 Postal Manual) Do Not Return

"The aeronautical and space activities of the United States shall be conducted so as to contribute . . . to the expansion of human knowledge of phenomena in the atmosphere and space. The Administration shall provide for the widest practicable and appropriate dissemination of information concerning its activities and the results thereof."

—NATIONAL AERONAUTICS AND SPACE ACT OF 1958

NASA SCIENTIFIC AND TECHNICAL PUBLICATIONS

TECHNICAL REPORTS: Scientific and technical information considered important, complete, and a lasting contribution to existing knowledge.

TECHNICAL NOTES: Information less broad in scope but nevertheless of importance as a contribution to existing knowledge.

TECHNICAL MEMORANDUMS: Information receiving limited distribution because of preliminary data, security classification, or other reasons. Also includes conference proceedings with either limited or unlimited distribution.

CONTRACTOR REPORTS: Scientific and technical information generated under a NASA contract or grant and considered an important contribution to existing knowledge.

TECHNICAL TRANSLATIONS: Information published in a foreign language considered to merit NASA distribution in English.

SPECIAL PUBLICATIONS: Information derived from or of value to NASA activities. Publications include final reports of major projects, monographs, data compilations, handbooks, sourcebooks, and special bibliographies.

TECHNOLOGY UTILIZATION PUBLICATIONS: Information on technology used by NASA that may be of particular interest in commercial and other non-aerospace applications. Publications include Tech Briefs, Technology Utilization Reports and Technology Surveys.

Details on the availability of these publications may be obtained from:

SCIENTIFIC AND TECHNICAL INFORMATION OFFICE

NATIONAL AERONAUTICS AND SPACE ADMINISTRATION

Washington, D.C. 20546